Interconversion between Parallel and Antiparallel Conformations of a 4H RNA junction in Domain 3 of Foot-and-Mouth Disease Virus IRES Captured by Dynamics Simulations

Segun Jung and Tamar Schlick*
Department of Chemistry and Courant Institute of Mathematical Sciences, New York University, New York, New York

ABSTRACT RNA junctions are common secondary structural elements present in a wide range of RNA species. They play crucial roles in directing the overall folding of RNA molecules as well as in a variety of biological functions. In particular, there has been great interest in the dynamics of RNA junctions, including conformational pathways of fully base-paired 4-way (4H) RNA junctions. In such constructs, all nucleotides participate in one of the four double-stranded stem regions, with no connecting loops. Dynamical aspects of these 4H RNAs are interesting because frequent interchanges between parallel and antiparallel conformations are thought to occur without binding of other factors. Gel electrophoresis and single-molecule fluorescence resonance energy transfer experiments have suggested two possible pathways: one involves a helical rearrangement via disruption of coaxial stacking, and the other occurs by a rotation between the helical axes of coaxially stacked conformers. Employing molecular dynamics simulations, we explore this conformational variability in a 4H junction derived from domain 3 of the foot-and-mouth disease virus internal ribosome entry site (IRES); this junction contains highly conserved motifs for RNA-RNA and RNA-protein interactions, important for IRES activity. Our simulations capture transitions of the 4H junction between parallel and antiparallel conformations. The interconversion is virtually barrier-free and occurs via a rotation between the axes of coaxially stacked helices with a transient perpendicular intermediate. We characterize this transition, with various interhelical orientations, by pseudodihedral angle and interhelical distance measures. The high flexibility of the junction, as also demonstrated experimentally, is suitable for IRES activity. Because foot-and-mouth disease virus IRES structure depends on long-range interactions involving domain 3, the perpendicular intermediate, which maintains coaxial stacking of helices and thereby consensus primary and secondary structure information, may be beneficial for guiding the overall organization of the RNA system in domain 3.

INTRODUCTION

Many exciting recent discoveries have transformed our understanding of RNA molecules far beyond the means of information transfer and protein synthesis (1–5). To perform specific biological functions, RNA molecules adopt well-defined three-dimensional (3D) structures in the cell (6–8). These 3D structures are formed by basic secondary structural elements like helices, hairpins, bulges, internal loops, and junctions. Although simple secondary structural elements such as hairpins and internal loops are well studied (9), our current understanding of complex RNA junctions is limited mainly due to their structural complexity and involvement in intricate long-range interactions.

An RNA junction serves as a hub for different double-stranded helical arms (10). Junctions are ubiquitous to species from small RNAs such as riboswitches, transfer RNAs, and hairpin ribozymes (11–13) to large ribosomal subunits (14,15) and viral RNAs (16,17). RNA junctions play crucial roles in RNA folding, serving as guides to the overall assembly of RNA molecules (18). Correspondingly, the structural, energetic, and dynamic aspects of junction motifs are important for our understanding on functional perspective of complex RNAs.

A growing amount of RNA structural data, obtained mainly from x-ray crystallography and NMR, has offered an exceptional opportunity to classify and explore structural properties of RNA junctions. The first nomenclature for nucleic acids classification of junctions was proposed by Lilley et al. (10) based on the number of helices and of connecting nucleotides at the branch point. Lescoute and Westhof (19) compiled and analyzed the 3-way junctions, classifying the topologies into three different families and formulating the rules of coaxial helical stacking formation; the coaxial stacking of helices is a common structural feature of the RNA junctions that maximizes base stacking. Laing et al. (20,21) extended the topology classification and analysis to study 4-way and higher-order junctions, grouping 4-way junctions into nine families based on coaxial stacking formation and overall helical arrangements. Bindewald et al. (22) developed the RNAJunction database, which provides several thousands of solved RNA junctions with detailed structural annotation. All these analyses, however, provide limited insights into the dynamic properties of RNA junctions.

Indeed, RNA junctions are dynamic structural entities, capable of undergoing conformational transitions. A prominent example is the 4-way RNA junction of hepatitis C virus (HCV) internal ribosome entry site (IRES), a specific RNA structure for internal translation initiation. The

Submitted October 7, 2013, and accepted for publication December 3, 2013.
*Correspondence: schlick@nyu.edu
Editor: Lois Pollack.

0006-3495/14/01/0447/12 $2.00
http://dx.doi.org/10.1016/j.bpj.2013.12.008

junction in HCV IRES is important in the overall IRES structure conformation. Two different conformations of the RNA junction were reported—parallel and antiparallel structures—by both crystallography and single-particle cryo-electron microscopy techniques (16,23). Later, Lilley et al. (24) studied the IRES RNA junction using comparative gel electrophoresis and fluorescence resonance energy transfer and showed that two different conformations can interconvert via continuous transitions (see Fig. 1 *C*).

Such dynamic characteristics of 4-way junctions often have functional significance. For example, the 4-way junction in U1 snRNA plays a crucial role in organizing the whole RNA molecule via RNA-RNA interactions (25,26); the junction in the hairpin ribozyme forms a catalytic site for the RNA self-cleavage reaction (27); and the junctions in viral mRNAs are essential for translating the maturation protein-encoding gene (28). All these 4-way junctions contain fully base paired four helical arms with no additional nucleotides at the point of strand exchange, an architecture termed 4H junction (10) (Fig. 1), also known as a Holiday junction in DNA (29).

These 4H junctions in RNA molecules exhibit similar coaxial stacking patterns as in DNA; however, they differ in global structure depending on the local sequence content at the branch point and the ionic strength. For example, 4H DNA junctions require metal ions for a compact fold by coaxially stacked helices and have a strong preference for antiparallel conformations. 4H RNA junctions, however, appear to fold by pairwise coaxial stacking of helices in the absence of metal ions (13,25,30) and are known to fluctuate between multiple conformations during the search for the most stable native structure (24,31–33). The conformational states of 4H RNA junctions consist of different helical stacking conformers with either parallel (AB, CD or AD, CB) or antiparallel (AB, DC, or AD, BC) arrangements (Fig. 1) (32). Although the mechanism of interconversion is not fully understood, the experimental data suggest two possibilities. One intermediate involves a helical rearrangement by (partial) unstacking of the helices, and another possibility is a rotation between helical axes while maintaining the stacked conformers intact (32).

Molecular dynamics (MD) simulations are a well-established method to investigate structural properties of biomolecules at an atomic level. Previous modeling and dynamics studies of large RNAs with junctions include riboswitches to investigate conformational dynamics upon

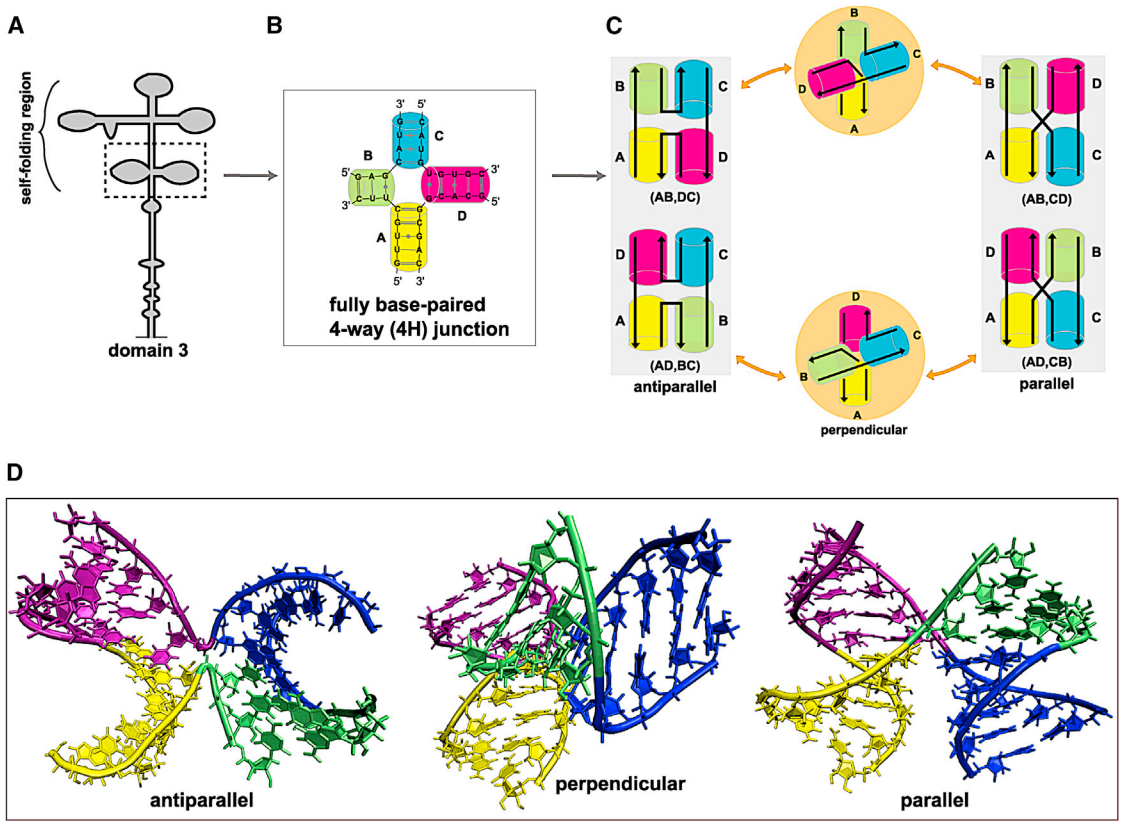

FIGURE 1 A fully base paired 4-way junction with possible conformations. (*A*) Schematic representation of domain 3 in FMDV IRES with a fully base-paired 4-way junction (4H junction) in the inset. (*B*) Secondary structure of the 4-way junction in domain 3, deduced from the RNA structure probing experiment. (*C*) A possible pathway of the 4H junction that can interconvert between parallel and antiparallel conformations via a perpendicular intermediate with alternative stacked conformers. (*D*) 3D models of the parallel, antiparallel, and a perpendicular intermediate captured in this work. To see this figure in color, go online.

substrate binding (34–36), ribosomal subunits to explore dynamic properties with respect to the biological functions (37,38), and viral RNAs to predict and characterize structural models (39,40). Domain 3 in foot-and-mouth disease virus (FMDV) IRES is the largest structural element containing multiple 4-way junctions. Its apical region, a self-folding RNA molecule, directs adjacent stem loops for correct RNA folding (41). Here, we investigate the ambient fluctuations of a free 4H junction found in FMDV IRES domain 3 (Fig. 1), by MD simulations. The sequence of the 4H junction is highly conserved, implying that its secondary structure is constrained under evolutionary pressure to deliver important biological functions (40). Indeed, the 4H junction provides potential binding motifs in helix D for RNA-RNA and RNA-protein interactions, crucial for IRES activity, involving the GNRA (N is any nucleotides; R is A or G) tetraloop and polyC binding protein (PCBP2), respectively (Fig. 2) (42). Thus, the dynamic characteristics and folding pathways of this 4H junction are important for understanding the junction's role in the folding and activity of domain 3.

Our simulations capture the transition dynamics and folding pathway of this IRES-associated 4H junction in domain 3. We observe a concerted, virtually barrier-free in terms of the potential energy (see Fig. S1 in the Supporting Material), transition from antiparallel (AD, BC) to perpendicular (AD⊥BC), and from perpendicular (AD⊥BC) to parallel (AD, CB) conformations, driven by a rotation between axes of the coaxially stacked helices (Fig. 3). During these interconversions, the pairwise coaxial stacking of helices remains intact. Our captured transitions in the MD trajectories exhibit various interhelical angles and involve a perpendicular intermediate, less stable than the two other conformations. Because the GNRA tetraloop-receptor long-range interactions are important for the folding of IRES, the transient perpendicular intermediate connecting the parallel and antiparallel configurations may be beneficial for overall IRES structure organization because the maintained coaxial stacks may help direct essential tertiary-contact formation.

MATERIAL AND METHODS

RNA target sequence and 3D structure modeling

Domain 3 of FMDV IRES is a self-assembling RNA that is 214 nt long. Using the sequence and secondary structure of truncated domain 3 in FMDV C-S8 IRES, we modeled 3D structures that include the 4H junction with three different system sizes—34, 45, and 116 nt (Fig. 2)—following the same modeling procedure described in our previous work (40).

In brief, we developed a computational divide-and-conquer strategy for modeling candidate tertiary structures for the IRES RNA (40). We began by modeling junction topology candidates and then built atomic 3D models consistent with available experimental data using MC-Sym (43), which uses a fragment-based library to obtain all possible RNA structures. Because fewer nucleotides between helices restrict the structural flexibility yielding coaxially stacked helices, no constraints were applied to yield stacked conformers. We modeled the 4H junction

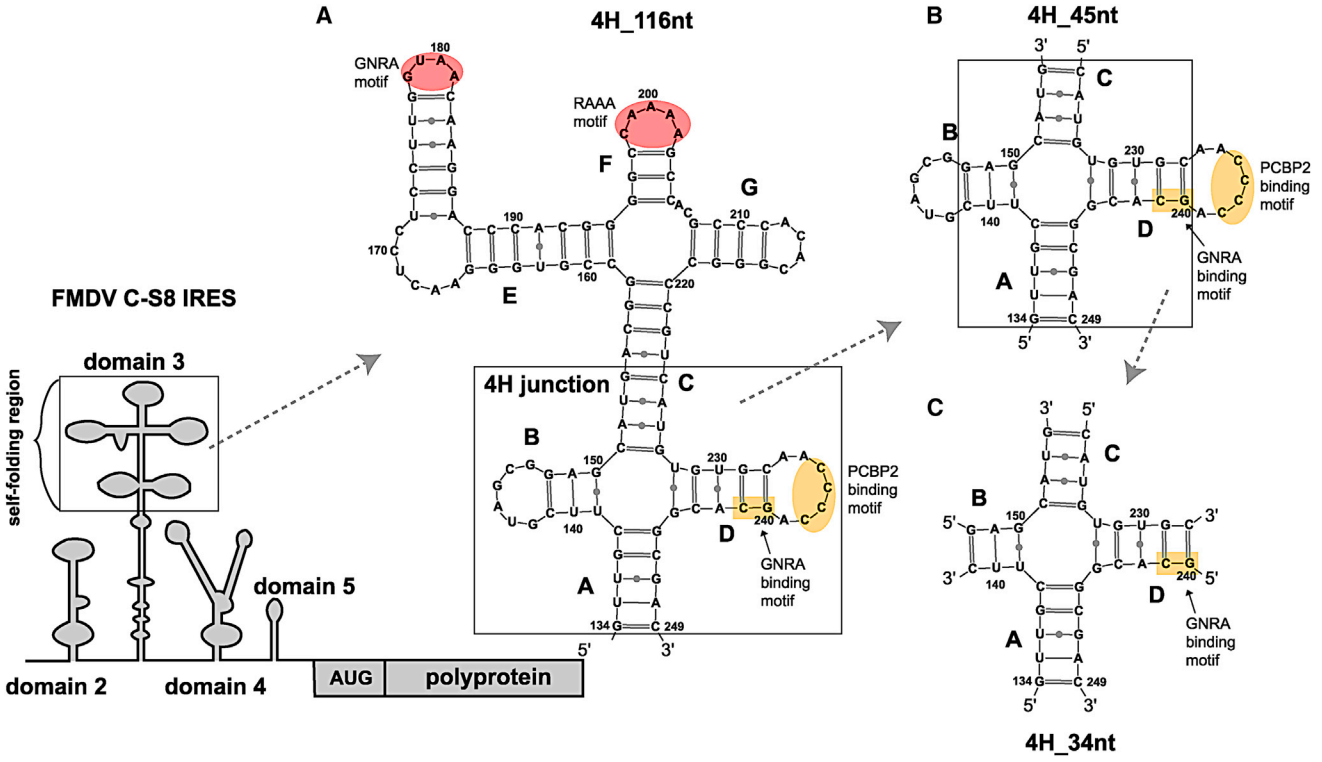

FIGURE 2 A secondary structure of domain 3 in FMDV C-S8 IRES. Three systems of truncated domain 3 with different sizes are prepared with a sequence length of 116 *nt* (*A*), 45 *nt* (*B*), and 34 *nt* (*C*). To see this figure in color, go online.

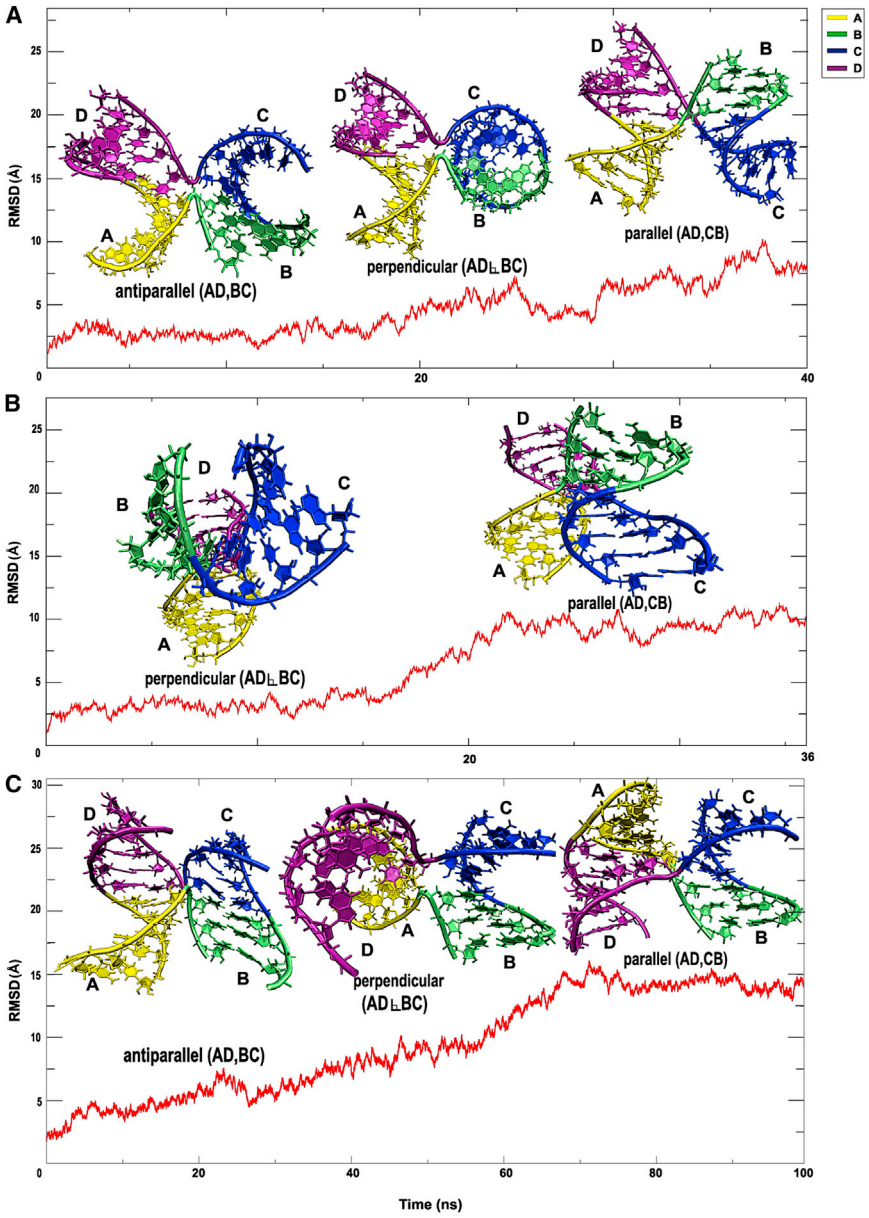

FIGURE 3 Conformational change of the 4H junction in FMDV IRES domain 3. While keeping pairwise coaxial stacking of helical arms intact, a transition from antiparallel or perpendicular to parallel states (simulation name: *Perp_34nt* (*A*), *Perp_45nt* (*B*), and *Anti_116nt_2* (*C*)) was observed, driven by a rotation between the helical axes. To see this figure in color, go online.

(G_{134},…, G_{145}, C_{224},…, C_{249}) by following the 5′-to-3′ direction without and with hairpin loops in the helices B and D to produce two different RNA systems (34 and 45 nt). To select final candidates corresponding to the three different conformations (parallel, perpendicular, and antiparallel), we used a clustering analysis followed by a visual inspection of representative structures from each cluster. We generated the remaining structural elements (A_{146},…,U_{223}), composed of a 4-way junction and a helix (U_{172},…,A_{187}), connected by a long bulge (A_{166},…,C_{171}). Specifically, the junction and helix were modeled separately by following the 5′-to-3′ direction, and then assembled via the long bulge. The large RNA system (116 nt) was modeled by combining these two structural entities—4H junction and the remaining structure—by imposing a distance constraint of 10 Å (between A_{180} and C_{232}-G_{240} using C1′ atoms) for the GNRA tetraloop-receptor long-range interactions. Similar to the previously mentioned smaller junction systems, final candidate structures were selected based on a clustering analysis and visual inspection. See Jung and Schlick (40) for full details.

Junction systems

We prepared three different sets of RNA systems differing by sizes and helical arrangements (Table 1 and Fig. 2). The first set, 34 nt, contains parallel (system name: *Para_34nt*), perpendicular (system name: *Perp_34nt*), and antiparallel (system name: *Anti_34nt*) configurations. The second set, 45 nt, consists of parallel (system name: *Para_45nt*), perpendicular (*Perp_45nt*), and antiparallel (system name: *Anti_45nt*) configurations. The third set, 116 nt, includes parallel (system name: *Para_116nt*) and antiparallel (system name: *Anti_116nt_1* and *Anti_116nt_2*) configurations with different stacking conformers, either D with A or B with A.

The RNA systems in the first set are composed of four helical arms without hairpin loops on helices B and D, whereas the second set contains hairpin loops that may form loop-helix or loop-loop tertiary interactions. The third set contains the 4H junction plus additional structural elements that could establish tertiary contacts in various forms including the long-range interactions involving the GNRA and RAAA motifs (Fig. 2).

TABLE 1 List of simulations of 4H RNA junctions in FMDV IRES domain 3

Simulation name	Size (nt)	Starting structure configuration	Force field	Trajectory length (ns)	Conformational change
Anti_34nt	34	Antiparallel (AB,DC)	bsc0χ_{OL3}	92	No transition
Perp_34nt	34	Perpendicular (AD,BC)	bsc0χ_{OL3}	40	Fluctuation between antiparallel and perpendicular, and transition from perpendicular to parallel
Para_34nt	34	Parallel (AB,CD)	bsc0χ_{OL3}	219	No transition
Anti_45nt	45	Antiparallel (AD,BC)	bsc0χ_{OL3}	104	No transition
Perp_45nt	45	Perpendicular (AD,BC)	bsc0χ_{OL3}	36	Transition from perpendicular to parallel
Para_45nt	45	Parallel (AD,BC)	bsc0χ_{OL3}	30	No transition
Anti_116nt_1	116	Antiparallel (AB,DC)	bsc0	100	No transition
Anti_116nt_2	116	Antiparallel (AD,BC)	bsc0	100	Transition from antiparallel to perpendicular, and from perpendicular to parallel
Para_116nt	116	Parallel (AB,CD)	bsc0	100	No transition

The name of the simulated structure is based on the three different systems shown in Fig. 2.

MD simulations

We solvated each system with the explicit TIP3P (44) water model in a water box of dimension 10 Å on each side using tLeap from the AmberTools package (45). Simulations were performed using the Amber parmbsc0 and parmbsc0χ_{OL3} force fields (46–49) with sodium ions to neutralize the system charge.

The choice of a force field for RNA is often crucial to achieve meaningful and reliable trajectories. We tested two latest Amber force fields, parmbsc0 and parmbsc0χ_{OL3}, for RNA—the latter representing an improved version of parmbsc0 for χ torsion angles. We found both force fields perform equally well for our simulated systems, not exhibiting any χ torsion angle related problems (50,51). However, we observed a base pair disruption at the helix end of B, formed by three base pairs without a hairpin loop, in our smallest RNA systems (*Anti_34nt* (~54 ns) and *Para_34nt* (~195 ns) in Table 1). This likely occurs because a helix composed of $\leq$3 base pairs may be too small to maintain the overall structural stability corresponding to the secondary structure.

We minimized each system in two steps, first over the water and ion molecules holding domain 3 fixed and, second, with all constraints removed. The minimization was performed using the Powell conjugate gradient algorithm (52). The initial equilibration was achieved over 60 ps at constant temperature (300 K) and pressure (1 atm), respectively. Pressure was maintained at 1 atm using the Langevin piston method, with a piston period of 100 fs, damping constant of 50 fs, and piston temperature of 300 K. Temperature coupling was enforced by velocity reassignment every 2 ps. Both minimization and equilibration were performed using the NAMD program (53).

For the production run, each system was simulated at constant temperature (300 K) and volume using weakly coupled Langevin dynamics of non-hydrogen atoms, with a damping coefficient of $c = 10\ \mathrm{ps}^{-1}$ with a 2-fs time step maintaining bonds to all hydrogen atoms rigid. Nonbonded interactions were truncated at 12 Å and 14 Å for van der Waals and electrostatic forces, respectively. Periodic boundary conditions were applied, and the particle mesh Ewald method was used to calculate electrostatic interactions.

All simulations using the NAMD package were run on the local clusters at New York University and the IBM Blue Gene/L supercomputer at the Computational Center for Nanotechnology Innovations (CCNI) based in Rensselaer Polytechnic Institute, NY.

Principal component analysis (PCA)

To identify the most significant conformational degrees of freedom of a system, dynamics trajectories of 4H junctions were analyzed using PCA (54). PCA describes the overall dynamics of systems with collective essential motion. The approach is based on the positional $n \times n$ (where $n = 3 \times$ number of atoms N) covariance matrix, C, defined as

$$\mathrm{C} = \left[(r_i - \langle r_i \rangle)(r_j - \langle r_j \rangle)\right],$$

where r_i and r_j are position vectors of two atoms i and j in the fitted structure and the angular brackets ($\langle ... \rangle$) denote the average over all sampled conformations. By diagonalizing the covariance matrix C, the eigenvectors, V, and their corresponding eigenvalues, λ, are obtained defined as

$$\mathrm{V}^{\mathrm{T}}\mathrm{CV} = \Lambda, \text{ or } \mathrm{CV}_{\mathrm{n}} = \lambda_{\mathrm{n}}\mathrm{V}_{\mathrm{n}},$$

where Λ is the diagonal matrix, diag $(\lambda_1, \lambda_2, ..., \lambda_{3N})$, with eigenvalues λ_i and $n = 1,2,\ldots,3N$.

To remove rotational and translational motions of the trajectory, we used the least squares method to fit the trajectories to its initial configuration as a reference structure. Each eigenvector $\mathrm{V_n}$ defines the direction of motion of N atoms as an oscillation about the average structure $\langle \mathrm{X} \rangle$. The normalized magnitude of the corresponding eigenvalue is a measure of the amplitudes of motion along the eigenvector $\mathrm{V_n}$ as calculated by $\lambda_{\mathrm{i}}/\sum_i \lambda_{\mathrm{i}}$ and organized in decreasing order. Thus, λ_1 represents the largest positional fluctuation and λ_n the least.

RESULTS

Global dynamic motions of the 4H junction

The 4H junction in FMDV IRES domain 3 (Fig. 1) is defined by the base sequence—C_{138}, U_{139},…, G_{149}, C_{150},…, G_{227}, U_{228},…, G_{244}, and G_{245}—for the four helical arms at the junction center. We label each helical arm by A through D following the 5′-to-3′ direction that consists of canonical Watson-Crick basepairs and three G-U wobble pairs (Fig. 1). Our starting 3D models of parallel, perpendicular, and antiparallel configurations contain pairwise coaxial stacking of helical arms as all 4H junctions studied experimentally (25).

The major folding pathway of the 4H junction suggested by experimental data (31,32) involves fluctuations between parallel and antiparallel configurations with two possible intermediates: one is via a helical rearrangement caused by partial or full unstacking of the helices due to insufficient cation binding to the junction; the other is via a rotation between axes of two stacking conformers (Fig. 1 *C*).

In our collective dynamics data for nine different systems (see Table 1), various helical arrangements of the junction

including parallel, perpendicular, and antiparallel are sampled. These conformations are all connected via a rotation between coaxially stacked helices, which exhibits various interhelical angles. Specifically, three simulated systems with different sizes of 34, 45, and 116 nt (simulation name: *Perp_34nt, Perp_45nt,* and *Anti_116nt_2* listed in Table 1) exhibit such transitions within ~6 ns: *Perp_34nt* shows fluctuation between antiparallel and perpendicular configurations, and a transition of perpendicular to parallel configurations followed by fluctuation between perpendicular and parallel states; *Perp_45nt* exhibits a transition from perpendicular to parallel conformations; and *Anti_116nt_2* fluctuates gradually from an antiparallel to a perpendicular intermediate followed by a transition from perpendicular to parallel states (Fig. 3).

The other six simulated systems remain in one conformation. The junctions are likely stabilized by coaxially stacked helices or tertiary interactions. Namely, the systems of *Anti_34nt*, *Para_34nt*, and *Anti_45nt* appear to be stabilized by pairwise coaxial stacking, whereas *Para_45nt*, *Anti_116nt_1*, and *Para_116nt* exhibit both coaxial stacking and RNA-RNA tertiary interactions involving helices B and D that restrain the junction. We analyze further the conformational changes below.

Dominant motion captured by PCA

PCA of the dynamics trajectories of the 4H junction captures the dominant collective motion that occurs during the conformational changes. The first four eigenvalues (denote as PC1,…, PC4) of the PCA capture 91% of the overall motion: PC1, 65%; PC2, 20%; PC3, 4%; and PC4, 2%. Fig. 4 shows that PC1 characterizes the transition of three different conformations (parallel, perpendicular, and antiparallel) achieved by a rotation of one stacked conformer against the other. PC2 describes a rotational motion similar to the PC1, but characterizing only the transition between perpendicular and parallel states. PC3 and PC4 capture local motions such as bending, stretching, and twisting within the stacked helices.

Analysis of conformational changes using various geometric measures

The leading dynamic motion of the 4H junction captured by PCA involves a key rotational motion of helical axes. We quantify this motion by following the rotational angle by measuring the pseudodihedral angle describing the relative orientation of residues—G_{137}, G_{229}, U_{226}, and U_{140}—considering two base pairs at the interhelical interface (Fig. 5 A), as well as interhelical distances using a pair of these residues during the simulation time (see Fig. 6 *A*).

Assessment of conformational changes by a pseudodihedral angle

We measure the pseudodihedral angle θ, defined by the phosphate backbone atoms of G_{137}(P)-G_{229}(P)-U_{226}(P)-U_{140}(P) (Fig. 5 *A*), to illustrate the conformational change. The three systems (Fig. 5, *B–D*), exhibit similar θ distribution for the transition from perpendicular to parallel configurations. All the systems sample the perpendicular (θ: 7–16°) and parallel (θ: 55–60°) states. The system *Perp_34nt* (Fig. 5 *B*) fluctuates between 35° and −15°

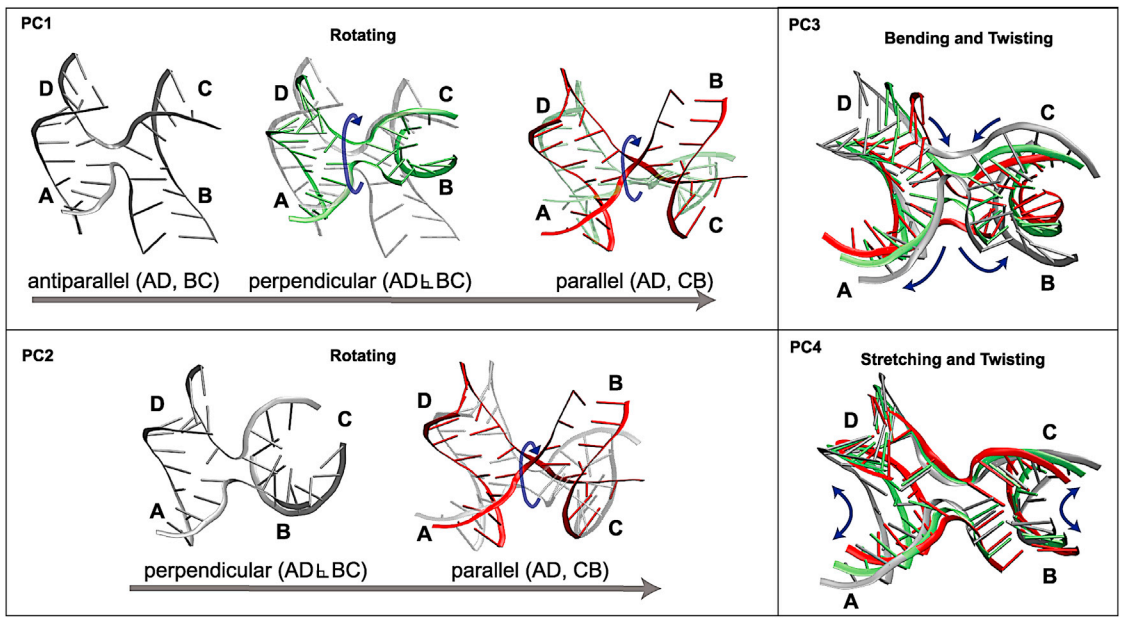

FIGURE 4 Major motions captured by PCA. PC1 and PC2 describe the global rotational motions of the 4H junction that transit structures from antiparallel to parallel forms and from perpendicular to parallel conformations, respectively; PC3 and PC4 capture the local bending and stretching motions of stacked helices, respectively. To see this figure in color, go online.

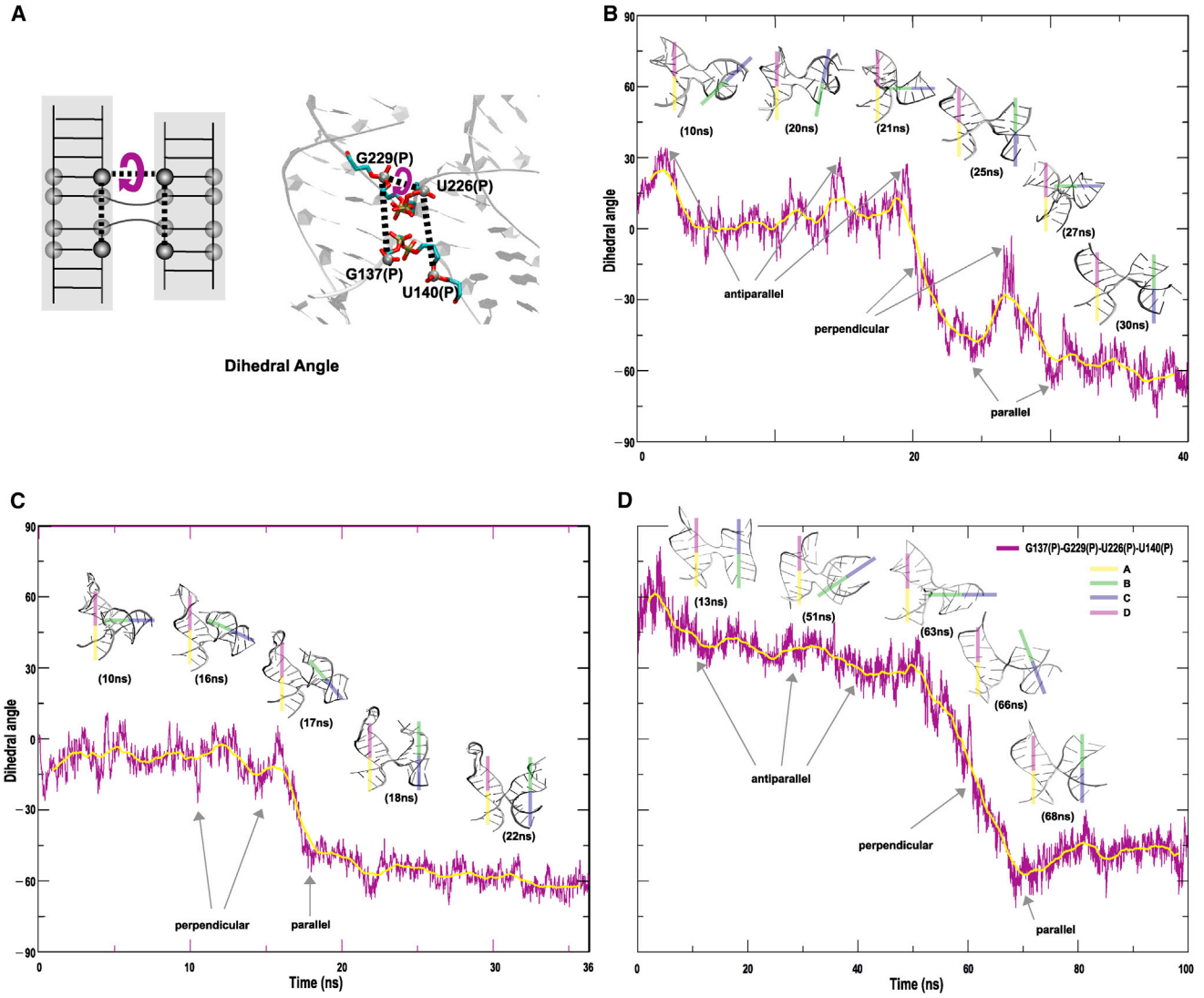

FIGURE 5 Conformational changes of the 4H junction described by a pseudodihedral angle between coaxially stacked helices using phosphate backbone atoms of the four residues G_{137}, U_{140}, U_{226}, and G_{229} near the center of the 4-way junction. (*A*) Representative definition of a pseudodihedral angle θ based on the four residues (G137, U140, U226, and G229 illustrated as *dark balls*) near the point of strand exchange involving the interhelical orientation in 2D structure (*left*) and the angle θ in the 3D structure (*right*). (*B*) The pseudodihedral angle sampled at every 20 ps over the 40 ns (*Perp_34nt*), 36 ns (*Perp_45nt*), and 100 ns (*Anti_116nt_2*) time course with some of the representative structures. To see this figure in color, go online.

over the first 19 ns, sampling a few antiparallel configurations followed by a rapid angle change from -15° to -56° within ~6 ns (from 19 to 25 ns) and arriving at a parallel configuration (25 ns). The system samples the perpendicular intermediate (27 ns) again and remains at the parallel state over the next 10 ns. *Perp_45nt* (Fig. 5 *C*) fluctuates with θ between 12° and -27° over the first 15 ns, fluctuating within a perpendicular state. Within the next 3 ns (from 15 to 18 ns), the system transitions from perpendicular to parallel states (18 ns) with the minimum θ of -56° and remains there over the next 18 ns. *Anti_116nt_2* (Fig. 5 *D*) gradually decreases during the antiparallel state from the maximum value of 81° to 30° over the first 50 ns where the average angle is $39.0 \pm 7.5^\circ$. Then, θ decreases rapidly to -71° over the next 18 ns (from 50 to 68 ns), exhibiting the conformational change from antiparallel to parallel configurations via a perpendicular intermediate; specifically, the system arrives at the perpendicular state (63 ns), and transitions from perpendicular to parallel states at 68 ns in ~5 ns. During the parallel conformation, the average θ is $-48.6 \pm 4.7^\circ$. Overall, the θ distribution shows three distinctive regions where two dominant states, parallel and antiparallel, are bridged by the perpendicular intermediate of the 4H junctions.

Assessment of conformational changes by interhelical distances

In Fig. 6 we measure two interhelical distances d1 and d2 defined by the backbone atoms of G_{137}(P)-U_{140}(P) and U_{226}(P)-G_{229}(P), respectively. Similar to the overall curve

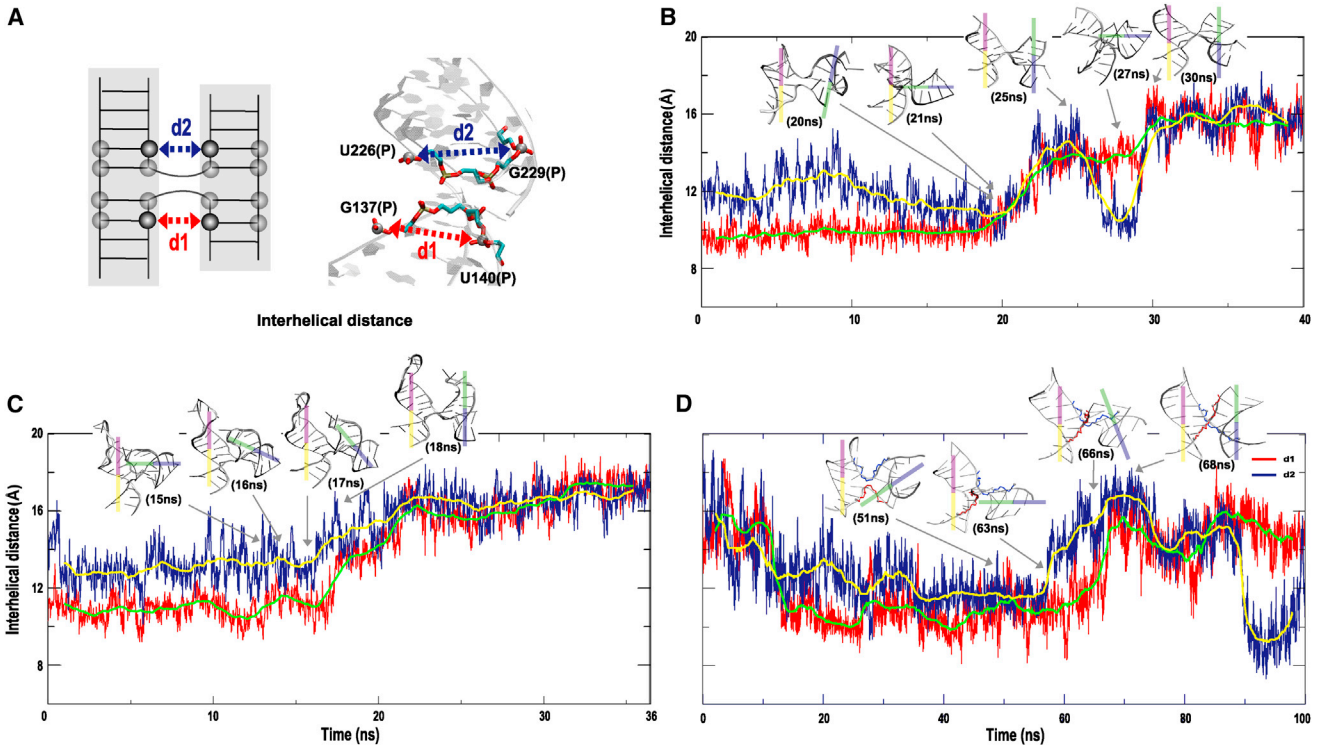

FIGURE 6 Conformational changes of the 4H junction described by interhelical distance between coaxially stacked helices. (*A*) Representative definition of the interhelical distances based on the four residues (G137, U140, U226, and G229 illustrated by *dark balls*) near the point of strand exchange in 2D (*left*) and in 3D (*right*). (*B*) Interhelical distances sampled at every 20 ps over the 40 ns (*Perp_34nt*), 36 ns (*Perp_45nt*), and 100 ns (*Anti_116nt_2*) time course with some representative structures around the rapid transition. To see this figure in color, go online.

of pseudodihedral angle, d1 and d2 of the three systems exhibit similar distances for the transition from perpendicular (10–13 Å) to parallel (14–16 Å) configurations. *Perp_34nt* (Fig. 6 *B*) shows that d2 converges to ~10 Å, whereas d1 is stable at ~10 Å (19 ns). Both d1 and d2 increase ~16 Å over the next 6 ns (19 to 25 ns). D2 only drops ~10 Å when the system samples again the perpendicular state at ~28 ns. *Perp_45nt* (Fig. 6 *C*) shows some fluctuations of d1 and d2 around 10 Å and 13 Å (15 ns), respectively. Both d1 and d2 increase ~14 Å over the next 3 ns (from 15 to 18 ns) and transit from perpendicular to parallel configurations. *Anti_116nt_2* (Fig. 6 *D*) shows that both d1 and d2 decrease from ~16–17 Å to ~11 Å over the first 50 ns, within the antiparallel configuration. Both distances then increase abruptly, reaching the maximum value of 16 Å over the next 18 ns. Interestingly, the d2 distance rapidly decreases ~90 ns where we observe a tertiary interaction between B and D. Overall, the two interhelical distances behave similarly, but with different degrees of fluctuations.

Correlation between a pseudodihedral angle and interhelical distances

The previous pseudodihedral angle and interhelical distances (Figs. 5 and 6) describe the global and local motions with respect to the different conformational states. To analyze these parameters' contribution to the conformational changes, we examine the correlation between the dihedral angle and interhelical distances in Fig. 7.

During the perpendicular state for ~19 ns, *Perp_34nt* (Fig. 7 *A*) also samples a few antiparallel states. Although both d1 and d2 converge to ~10 Å, θ fluctuates between 35° and −15°. When θ decreases from −15° to −56° and both d1 and d2 increase ~16 Å, a transition occurs from perpendicular to parallel configurations within ~6 ns. *Perp_45nt* (Fig. 7 *B*) fluctuates during the perpendicular state (15 ns) with θ between 12° and −27°, and d1 and d2 each around 10 Å and 13 Å. With the decrease of θ from −27° to −56°, a transition occurs from perpendicular to parallel configurations within ~6 ns, whereas both d1 and d2 increase to ~16 Å. During the antiparallel conformation, which lasts for ~50 ns, both d1 and d2 of *Anti_116nt_2* (Fig. 7 *C*) arrive at a local minima of ~11Å, whereas θ gradually decreases to ~30°. From 30° to −30°, a rapid transition occurs from antiparallel to perpendicular states over 13 ns, whereas both d1 and d2 gradually increase. When θ is between −30° and −71°, the system achieves the parallel conformation with a maximum distance of ~16–17Å. During the parallel state, d2 fluctuates >d1 within the range of 7–18 Å and 10–17 Å, respectively, showing a scattered distribution. Interestingly, the overall trend of the correlated distribution

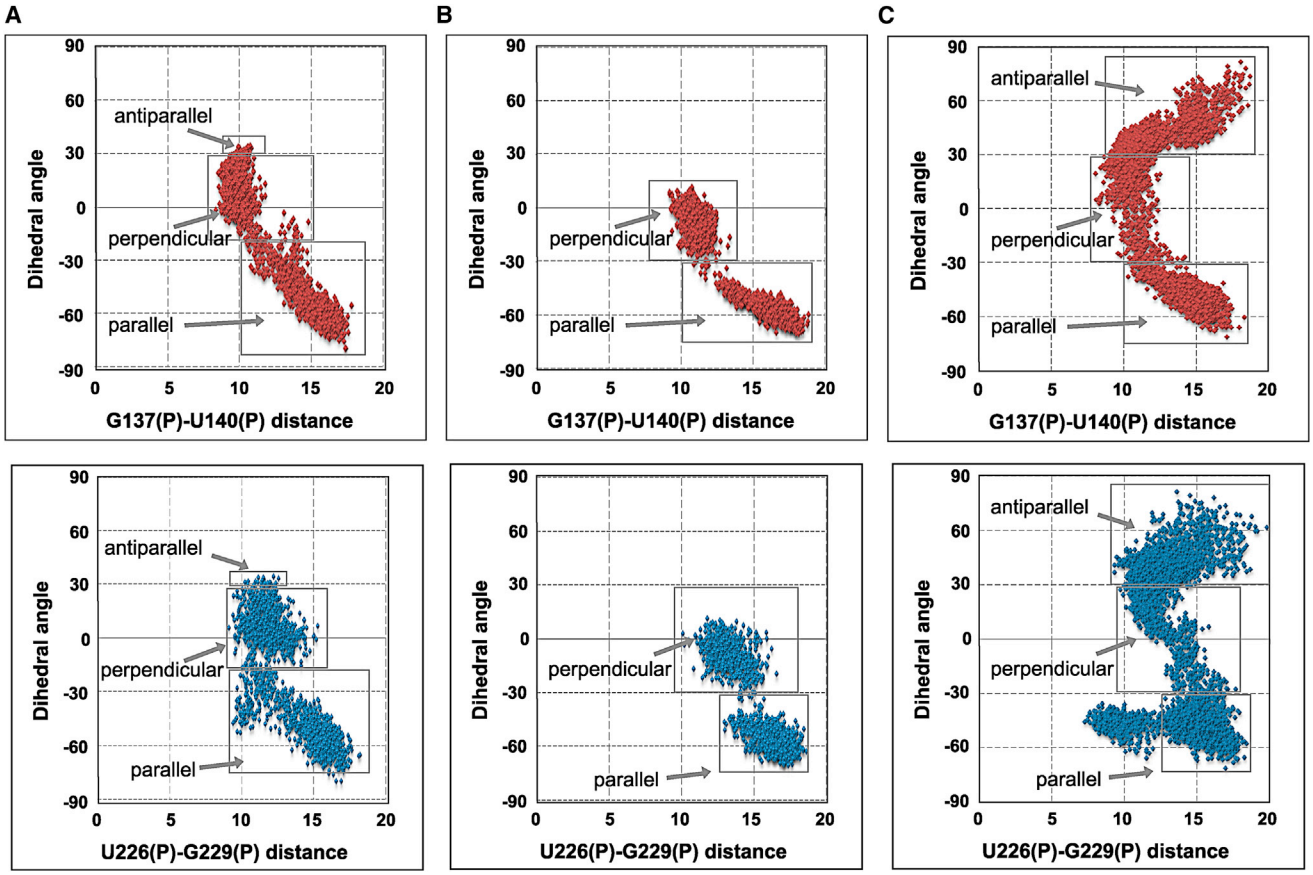

FIGURE 7 Overall distribution of the correlation between pseudodihedral angle and interhelical distances for the conformational change from perpendicular (*Perp_34nt* and *Perp_45nt*) and antiparallel (*Anti_116nt_2*) to parallel. A relation between the dihedral angle and the distances U_{226}(P)-G_{229}(P) and G_{137}(P)-U_{140}(P) for *Perp_34nt* (*A*), *Perp_45nt* (*B*), and *Anti_116nt_2* (*C*) is highlighted with solid gray boxes for these events (*parallel, perpendicular, and antiparallel configurations*). To see this figure in color, go online.

for θ versus d1 and d2 are similar. The difference at the parallel state of θ versus d2 is due to the tertiary contact between B and D, initiated at ~90 ns.

Flexibility of terminal basepairs at the core of the 4H junction

All basepairs in the 4H junction are involved with base pairing and stacking interactions, between complementary strands and between adjacent bases, respectively. For example, these interactions contribute significantly to RNA structure stability by forming coaxial helical stacks. Previously, a disruption of base stacking in the connecting (or interhelical) residues at the center of a RNA-DNA hybrid 4H junction was noted as responsible for achieving a different conformational state (33). Thus, we next analyze these base pairing and stacking interactions at the core of our 4H junction to assess their involvement with the conformational change from antiparallel to parallel configurations (*Anti_116nt_2*).

First, we measure distances of the base pairs at the helix ends—C_{138}-G_{245}, U_{139}-G_{150}, C_{151}-G_{227}, and U_{228}-G_{244}—around the junction center (or branch point) by considering nitrogen and oxygen atoms (Fig. S2). The four terminal basepairs consist of a pair of G-C and G-U bases. The latter (G-U) is thermodynamically less stable than the former (G-C). Fig. S2 shows that G-C basepairs in A and C remain highly stable with the average distance of 2.82 ± 0.07Å, whereas G-U wooble basepairs in B and D exhibit small fluctuations with average distances of 2.89 ± 0.12Å and 2.85 ± 0.09Å, respectively. In particular, fluctuations of the G-U basepair in D indicate that the hydrogen bonds are temporarily disrupted, affecting the basepairing and overall flexibility. All four basepairs maintain well the hydrogen bonds over the time course of the simulation.

Second, we measure in Fig. S3 base stacking interactions for the two nonconsecutive bases C_{138}-U_{228} and U_{139}-G_{227} between AD and BC, respectively. To consider base stacking interactions, we use geometric criteria of a distance ($\leq$5.5 Å) and angle ($\leq$30°) between these bases. Overall, the base stacking interactions are well maintained, with only temporary disruption during the antiparallel state. In particular, the base stacking interactions remain stable during the fast transition, from perpendicular to parallel configurations.

DISCUSSION

RNA junctions are the largest secondary structural element or motif found in diverse RNA molecules. They are structurally and functionally important, playing central roles in RNA folding. The 4H junction we examine here is the simplest type of a 4-way junction that contains fully base-paired helices often found in self-assembling molecules such as the hairpin ribozyme (27) and viral mRNAs (28). The junction's overall shape contributes significantly to biological functions (e.g., splicing, catalyzing, and translation initiation).

In general, 4H junctions in nucleic acids adopt well-defined helical arrangements that guide the overall fold via coaxial stacking interactions (55). The overall conformation of both 4H DNA and RNA junctions depends on the ion concentration. Although 4H DNA junctions reveal a preference for antiparallel conformations, 4H RNA junctions can adopt both parallel and antiparallel states. Gel electrophoresis and (single-molecule) fluorescence resonance energy transfer have suggested two possible pathways between parallel and antiparallel configurations: 1), a transition via a helical rearrangement by disrupting coaxial helical stacking; 2), a transition driven by a rotation at the center of the junction that maintains the coaxial stacks.

Using MD simulations, we have explored structural properties of the 4H junction, taken from FMDV IRES domain 3. This 4H junction brings together the distant RNA-RNA segments that play crucial roles in the structural stability and organization of the entire domain 3, which in turn affects IRES activity. Thus, assembly of the 4H RNA junction is a prerequisite for establishing the folded 3D structure of domain 3 and thus enabling the initiation mechanism of translation in FMDV IRES. Our studies suggest that both parallel and antiparallel configurations of the 4H junction are sampled, with a virtually barrier-free transition (Fig. S1) between them as deduced experimentally (32). The transition between parallel and antiparallel conformations occurs via a perpendicular intermediate that maintains the coaxial stacks (Fig. 1). Because the GNRA motif interacts with the helix D in the 4H junction, a transition that offers various stable configurations via pairwise coaxial stacking of helices is beneficial to initiate the long-range RNA-RNA interactions. Still, we cannot exclude other pathways for the transition.

Analysis of the principal motions indicates that both global and local motions contribute to the previous conformational exchanges. The first two largest PCs capture 85% of the dominant motion and characterize the transition between parallel and antiparallel via perpendicular states involving a rotation. The third and fourth largest PCs, in total of 6%, capture local motions within stacked helices (e.g., bending, stretching, and twisting). These motions are described by interhelical residues connecting the two coaxial stacking helices (Fig. 5 *A* and Fig. 6 *A*). Specifically, analysis of interhelical distances and pseudodihedral angles help organize the conformations into antiparallel, parallel, and perpendicular states and reveal the transience of the transition state. The polymorphic nature of the 4H junction without added cofactors is well appreciated in the literature (24,32) and thought to be advantageous for IRES's versatile functions. Thus, a modular structural platform that is easily adjusted by the binding of the molecular cofactors suits this large RNA for its complex activity.

The alternative suggested interconversion via a helical rearrangement, including a cruciform intermediate triggered by reduced cation binding at the junction domain, was not observed in our equilibrium trajectories within the 30–100 ns timescale, neutralized by Na^+ ions; the pairwise coaxial stacks of helices remain intact due to effective screening of the strong Coulomb repulsion between RNA junction domains. It is important to note that simulations of RNA structures may be sensitive to ionic conditions in the sense that different conditions may favor certain folds. Indeed, previous molecular simulations on RNA systems have shown that different results were achieved using net-neutralizing K^+ cations on one hand versus excess K^+ cations on the other (56); however, no difference was observed when Na^+ cations were applied using different ionic concentrations (e.g., net-neutralizing Na^+ versus 0.2 and 0.35 M excess salt) (37,57,58). In addition, state-of-the-art nucleic acids force fields for MD simulations describe well-monovalent ions and solute-solvent interactions, but not divalent ions (59). Progress continues on these fronts.

The perpendicular intermediate, in particular, may be advantageous for directing further long-range RNA-RNA interactions via the GNRA or RAAA motifs because it provides a rapid transition that can potentially accelerate assembly of interactions with a possible binding site in the 4H junction. It is possible that although one of the coaxially stacked helices is occupied in tertiary interactions in the perpendicular orientation, the other stacked conformer continues to explore conformational space to find its tertiary interaction partner for further stabilization. Ultimately, we envision that inter- and intramolecular RNA-RNA interactions, possibly involving the hairpin loops in helices B and D, are required to anchor the 4H junction in either the parallel or antiparallel conformation.

SUPPORTING MATERIAL

Three figures are available at http://www.biophysj.org/biophysj/supplemental/S0006-3495(13)05795-0.

We thank Dr. Mai Zahran for discussions.

This work is supported by National Science Foundation (EMT award CCF-0727001 to T.S.); National Institutes of Health (grants GM081410 and GM100469 to T.S.); and a MacCracken Fellowship to S.J. Funding for open access charge: National Science Foundation, National Institutes of Health.

The computations were made possible by support of the IBM Blue Gene/L supercomputer at the Computational Center for Nanotechnology Innovations (CCNI) based in Rensselaer Polytechnic Institute, NY. Molecular images were generated using the VMD program (60) and Gromacs tool packages (61) were used to analyze the dynamics data.

REFERENCES

1. Derrien, T., R. Johnson, …, R. Guigó. 2012. The GENCODE v7 catalog of human long noncoding RNAs: analysis of their gene structure, evolution, and expression. *Genome Res.* 22:1775–1789.
2. Gorodkin, J., and I. L. Hofacker. 2011. From structure prediction to genomic screens for novel non-coding RNAs. *PLOS Comput. Biol.* 7:e1002100.
3. Meyer, M. M., T. D. Ames, …, R. R. Breaker. 2009. Identification of candidate structured RNAs in the marine organism '*Candidatus Pelagibacter ubique*'. *BMC Genomics.* 10:268.
4. Will, S., M. Yu, and B. Berger. 2013. Structure-based whole-genome realignment reveals many novel noncoding RNAs. *Genome Res.* 23:1018–1027.
5. Weinberg, Z., J. X. Wang, …, R. R. Breaker. 2010. Comparative genomics reveals 104 candidate structured RNAs from bacteria, archaea, and their metagenomes. *Genome Biol.* 11:R31.
6. Hannon, G. J. 2002. RNA interference. *Nature.* 418:244–251.
7. Huysmans, F. T., H. W. van Hamersvelt, …, R. A. Koene. 1992. Acute renal effects of felodipine in hypertensive patients with kidney disease. *Kidney Int. Suppl.* 36:S106–S109.
8. Schroeder, R., A. Barta, and K. Semrad. 2004. Strategies for RNA folding and assembly. *Nat. Rev. Mol. Cell Biol.* 5:908–919.
9. Hendrix, D. K., S. E. Brenner, and S. R. Holbrook. 2005. RNA structural motifs: building blocks of a modular biomolecule. *Q. Rev. Biophys.* 38:221–243.
10. Lilley, D. M., R. M. Clegg, …, P. J. Hagerman. 1995. A nomenclature of junctions and branchpoints in nucleic acids. *Nucleic Acids Res.* 23:3363–3364.
11. Batey, R. T., S. D. Gilbert, and R. K. Montange. 2004. Structure of a natural guanine-responsive riboswitch complexed with the metabolite hypoxanthine. *Nature.* 432:411–415.
12. Kim, S. H., J. L. Sussman, …, A. Rich. 1974. The general structure of transfer RNA molecules. *Proc. Natl. Acad. Sci. USA.* 71:4970–4974.
13. Murchie, A. I., J. B. Thomson, …, D. M. Lilley. 1998. Folding of the hairpin ribozyme in its natural conformation achieves close physical proximity of the loops. *Mol. Cell.* 1:873–881.
14. Cate, J. H., M. M. Yusupov, …, H. F. Noller. 1999. X-ray crystal structures of 70S ribosome functional complexes. *Science.* 285:2095–2104.
15. Noller, H. F. 2005. RNA structure: reading the ribosome. *Science.* 309:1508–1514.
16. Kieft, J. S., K. Zhou, …, J. A. Doudna. 2002. Crystal structure of an RNA tertiary domain essential to HCV IRES-mediated translation initiation. *Nat. Struct. Biol.* 9:370–374.
17. Pilipenko, E. V., V. M. Blinov, …, V. I. Agol. 1989. Conservation of the secondary structure elements of the 5′-untranslated region of cardio- and aphthovirus RNAs. *Nucleic Acids Res.* 17:5701–5711.
18. Chastain, M., and I. Tinoco, Jr. 1991. Structural elements in RNA. *Prog. Nucleic Acid Res. Mol. Biol.* 41:131–177.
19. Lescoute, A., and E. Westhof. 2006. Topology of three-way junctions in folded RNAs. *RNA.* 12:83–93.
20. Laing, C., and T. Schlick. 2009. Analysis of four-way junctions in RNA structures. *J. Mol. Biol.* 390:547–559.
21. Laing, C., S. Jung, …, T. Schlick. 2009. Tertiary motifs revealed in analyses of higher-order RNA junctions. *J. Mol. Biol.* 393:67–82.
22. Bindewald, E., R. Hayes, …, B. A. Shapiro. 2008. RNAJunction: a database of RNA junctions and kissing loops for three-dimensional structural analysis and nanodesign. *Nucleic Acids Res.* 36 (Database issue):D392–D397.
23. Boehringer, D., R. Thermann, …, H. Stark. 2005. Structure of the hepatitis C virus IRES bound to the human 80S ribosome: remodeling of the HCV IRES. *Structure.* 13:1695–1706.
24. Melcher, S. E., T. J. Wilson, and D. M. Lilley. 2003. The dynamic nature of the four-way junction of the hepatitis C virus IRES. *RNA.* 9:809–820.
25. Duckett, D. R., A. I. Murchie, and D. M. Lilley. 1995. The global folding of four-way helical junctions in RNA, including that in U1 snRNA. *Cell.* 83:1027–1036.
26. Branlant, C., A. Krol, …, M. Jacob. 1981. The conformation of chicken, rat and human U1A RNAs in solution. *Nucleic Acids Res.* 9:841–858.
27. Hampel, A., and R. Tritz. 1989. RNA catalytic properties of the minimum (-)sTRSV sequence. *Biochemistry.* 28:4929–4933.
28. Poot, R. A., N. V. Tsareva, …, J. van Duin. 1997. RNA folding kinetics regulates translation of phage MS2 maturation gene. *Proc. Natl. Acad. Sci. USA.* 94:10110–10115.
29. Holliday, R. 2007. A mechanism for gene conversion in fungi. *Genet. Res.* 89:285–307.
30. Walter, F., A. I. Murchie, …, D. M. Lilley. 1998. Global structure of four-way RNA junctions studied using fluorescence resonance energy transfer. *RNA.* 4:719–728.
31. Tan, E., T. J. Wilson, …, T. Ha. 2003. A four-way junction accelerates hairpin ribozyme folding via a discrete intermediate. *Proc. Natl. Acad. Sci. USA.* 100:9308–9313.
32. Hohng, S., T. J. Wilson, …, T. Ha. 2004. Conformational flexibility of four-way junctions in RNA. *J. Mol. Biol.* 336:69–79.
33. Nowakowski, J., P. J. Shim, …, G. F. Joyce. 2000. Alternative conformations of a nucleic acid four-way junction. *J. Mol. Biol.* 300:93–102.
34. Villa, A., J. Wöhnert, and G. Stock. 2009. Molecular dynamics simulation study of the binding of purine bases to the aptamer domain of the guanine sensing riboswitch. *Nucleic Acids Res.* 37:4774–4786.
35. Priyakumar, U. D., and A. D. MacKerell, Jr. 2010. Role of the adenine ligand on the stabilization of the secondary and tertiary interactions in the adenine riboswitch. *J. Mol. Biol.* 396:1422–1438.
36. Huang, W., J. Kim, …, F. Aboul-ela. 2013. The impact of a ligand binding on strand migration in the SAM-I riboswitch. *PLOS Comput. Biol.* 9:e1003069.
37. Besseová, I., K. Réblová, …, J. Sponer. 2010. Molecular dynamics simulations suggest that RNA three-way junctions can act as flexible RNA structural elements in the ribosome. *Nucleic Acids Res.* 38:6247–6264.
38. Chen, K., J. Eargle, …, Z. Luthey-Schulten. 2012. Assembly of the five-way junction in the ribosomal small subunit using hybrid MD-Gō simulations. *J. Phys. Chem. B.* 116:6819–6831.
39. Perard, J., C. Leyrat, …, M. Jamin. 2013. Structure of the full-length HCV IRES in solution. *Nat. Commun.* 4:1612.
40. Jung, S., and T. Schlick. 2013. Candidate RNA structures for domain 3 of the foot-and-mouth-disease virus internal ribosome entry site. *Nucleic Acids Res.* 41:1483–1495.
41. Fernández, N., A. García-Sacristán, …, E. Martínez-Salas. 2011. Structural analysis provides insights into the modular organization of picornavirus IRES. *Virology.* 409:251–261.
42. Fernández-Miragall, O., R. Ramos, …, E. Martínez-Salas. 2006. Evidence of reciprocal tertiary interactions between conserved motifs involved in organizing RNA structure essential for internal initiation of translation. *RNA.* 12:223–234.
43. Parisien, M., and F. Major. 2008. The MC-Fold and MC-Sym pipeline infers RNA structure from sequence data. *Nature.* 452:51–55.
44. Jorgensen, W. L., J. Chandrasekhar, …, M. L. Klein. 1983. Comparison of simple potential functions for simulating liquid water. *J. Chem. Phys.* 79:926–935.
45. Case, D. A., T. A. Darden, …, P. A. Kollman. 2012. AMBER 12. University of California, San Francisco, CA.

46. Pérez, A., I. Marchán, …, M. Orozco. 2007. Refinement of the AMBER force field for nucleic acids: improving the description of alpha/gamma conformers. *Biophys. J.* 92:3817–3829.

47. Cornell, W. D., P. Cieplak, …, P. A. Kollman. 1995. A second generation force field for the simulation of proteins, nucleic acids, and organic molecules. *J. Am. Chem. Soc.* 117:5179–5197.

48. Zgarbová, M., M. Otyepka, …, P. Jurečka. 2011. Refinement of the Cornell et al. nucleic acids force field based on reference quantum chemical calculations of glycosidic torsion profiles. *J. Chem. Theory Comput.* 7:2886–2902.

49. Yildirim, I., S. D. Kennedy, …, D. H. Turner. 2012. Revision of AMBER torsional parameters for RNA improves free energy predictions for tetramer duplexes with GC and iGiC base pairs. *J. Chem. Theory Comput.* 8:172–181.

50. Mlýnský, V., P. Banás, …, M. Otyepka. 2010. Extensive molecular dynamics simulations showing that canonical G8 and protonated A38H+ forms are most consistent with crystal structures of hairpin ribozyme. *J. Phys. Chem. B.* 114:6642–6652.

51. Réblová, K., J. Sponer, and F. Lankas. 2012. Structure and mechanical properties of the ribosomal L1 stalk three-way junction. *Nucleic Acids Res.* 40:6290–6303.

52. Powell, M. J. D. 1964. An efficient method for finding the minimum of a function of several variables without calculating derivatives. *Comput. J.* 7:155–162.

53. Phillips, J. C., R. Braun, …, K. Schulten. 2005. Scalable molecular dynamics with NAMD. *J. Comput. Chem.* 26:1781–1802.

54. Amadei, A., A. B. Linssen, and H. J. Berendsen. 1993. Essential dynamics of proteins. *Proteins.* 17:412–425.

55. Lilley, D. M. 2000. Structures of helical junctions in nucleic acids. *Q. Rev. Biophys.* 33:109–159.

56. Besseová, I., M. Otyepka, …, J. Sponer. 2009. Dependence of A-RNA simulations on the choice of the force field and salt strength. *Phys. Chem. Chem. Phys.* 11:10701–10711.

57. Rázga, F., M. Zacharias, …, J. Sponer. 2006. RNA kink-turns as molecular elbows: hydration, cation binding, and large-scale dynamics. *Structure.* 14:825–835.

58. Spacková, N., K. Réblová, and J. Sponer. 2010. Structural dynamics of the box C/D RNA kink-turn and its complex with proteins: the role of the A-minor 0 interaction, long-residency water bridges, and structural ion-binding sites revealed by molecular simulations. *J. Phys. Chem. B.* 114:10581–10593.

59. McDowell, S. E., N. Spacková, …, N. G. Walter. 2007. Molecular dynamics simulations of RNA: an in silico single molecule approach. *Biopolymers.* 85:169–184.

60. Humphrey, W., A. Dalke, and K. Schulten. 1996. VMD: visual molecular dynamics. *J. Mol. Graph.* 14:33–38, 27–38.

61. Van Der Spoel, D., E. Lindahl, …, H. J. Berendsen. 2005. GROMACS: fast, flexible, and free. *J. Comput. Chem.* 26:1701–1718.

SUPPORTING MATERIAL

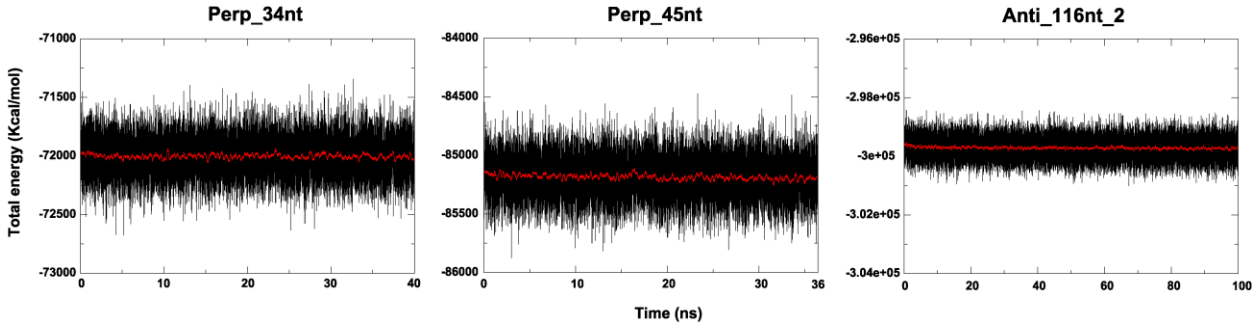

Figure S1. Total energy of the three different systems—*Perp_34nt* **(A)**, *Perp_45nt* **(B)**, and *Anti_116nt_2* **(C)**—that exhibit conformational changes. The red line shows an average value sampled at every 200 ps.

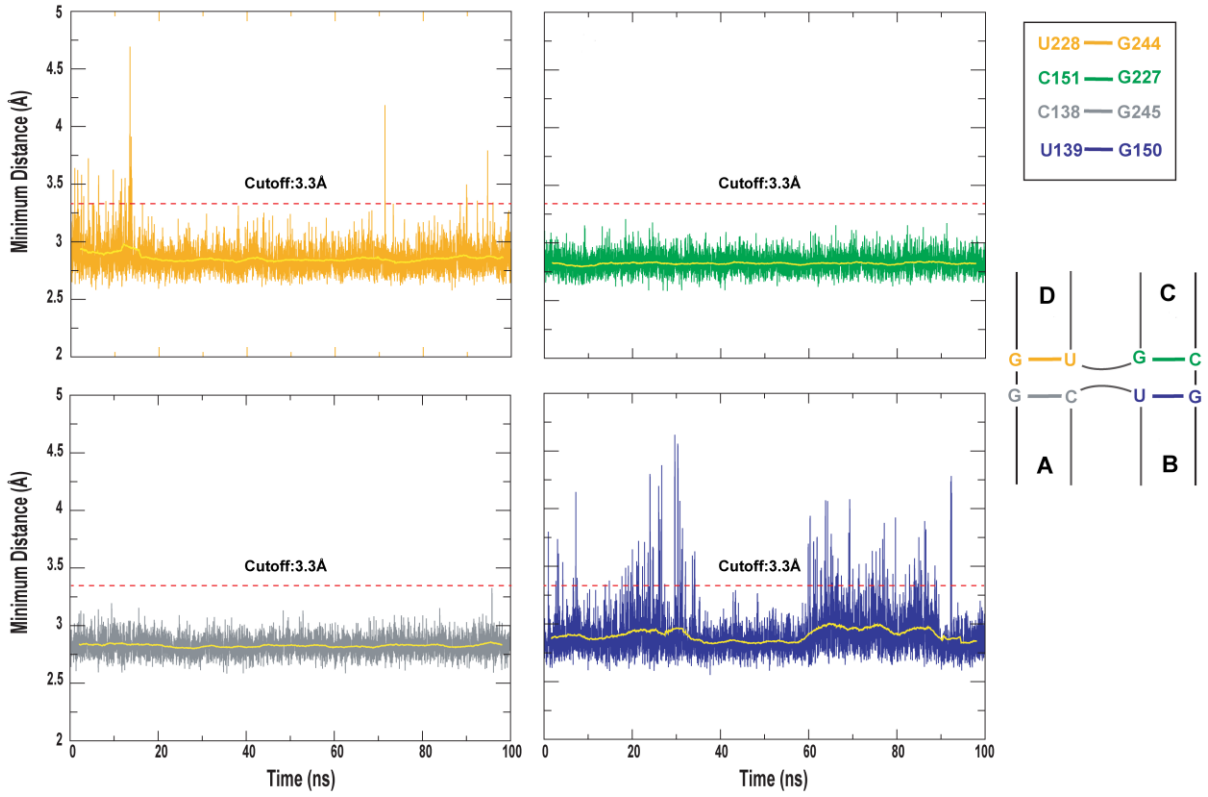

Figure S2. Distances of heavy atoms in terminal base pairs at the center of the 4H junction. While the distances of G-C base pairs in A (lower left) and C (upper right) are highly stable, the distances of G-U base pairs in B (lower right) and D (upper left) exhibit some fluctuations.

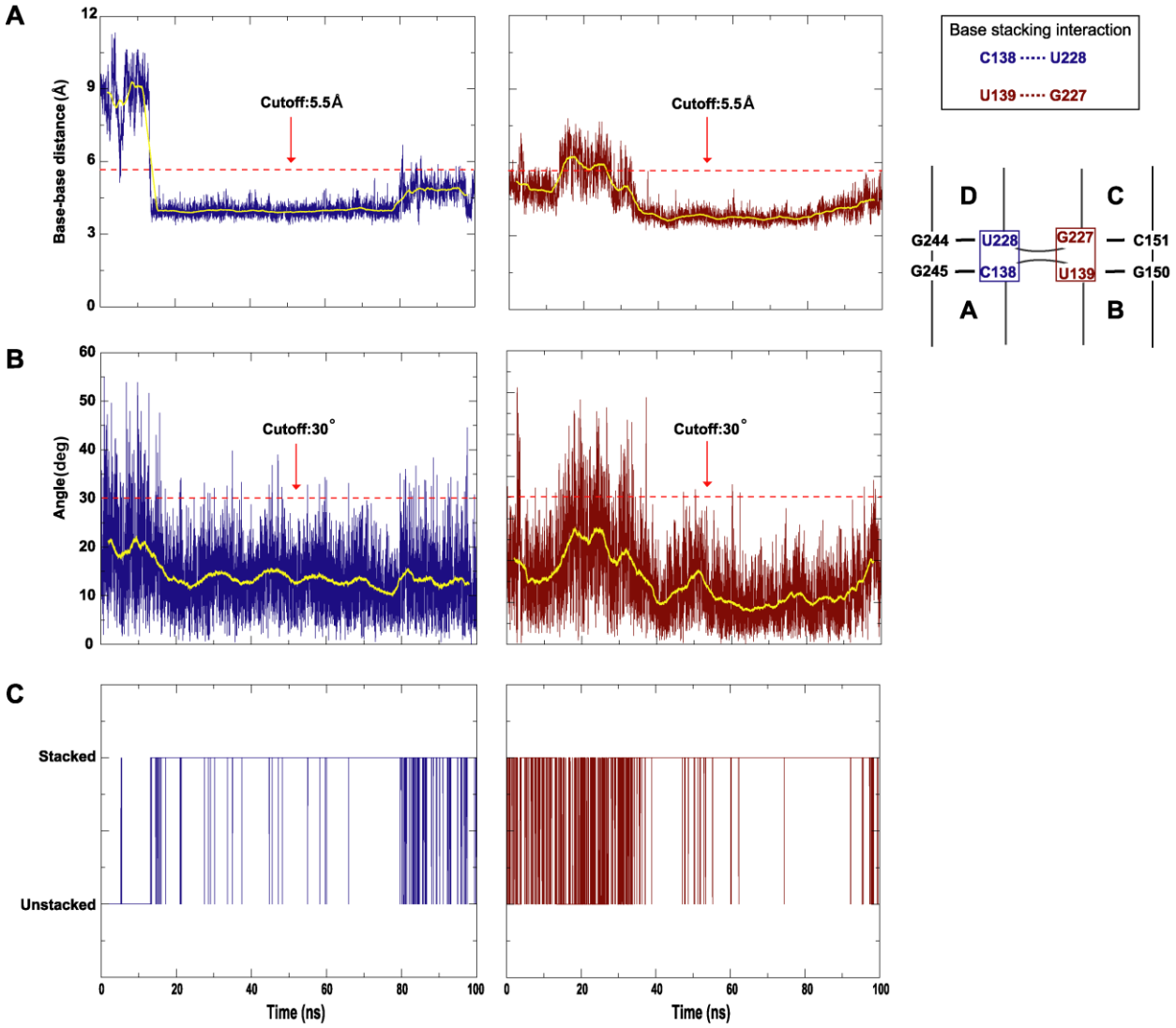

Figure S3. Base stacking interactions assessed by several measures. **(A)** Base-base distances less than or equal to 5.5 Angstroms. **(B)** An angle between adjacent bases lower than or equal to 30 degrees. **(C)** Base stacking interaction satisfying the distance and angle criteria above.